

# Modelling irradiance variations from the surface distribution of the solar magnetic field

M. Fligge<sup>1</sup>, S.K. Solanki<sup>1,2</sup>, and Y.C. Unruh<sup>3</sup>

<sup>1</sup> Institute of Astronomy, ETH-Zentrum, 8092 Zürich, Switzerland

<sup>2</sup> Max-Planck-Institut für Aeronomie, 37191 Katlenburg-Lindau, Germany

<sup>3</sup> Universität Wien, Astronomisches Institut, Türkenschanzstrasse 17, 1180 Wien, Austria

Received 6 May 1999 / Accepted 26 October 1999

**Abstract.** An important question in solar physics is to what extent solar surface magnetism affects the solar irradiance. Previous attempts to answer this question have employed proxies of the magnetic field to reconstruct the irradiance and compare it with observations. Here we present the first model calculations of solar irradiance variations based on variations of the surface distribution of the solar magnetic field. The irradiance reconstruction makes use of sunspot and facular contrasts calculated as a function of wavelength and limb angle on the Sun. The position and size of magnetic features on the solar disk are extracted from full-disk magnetograms obtained by the Michelson Doppler Interferometer (MDI) onboard the SOHO spacecraft.

The reconstructed spectral irradiance variations are compared with total and spectral contrast measurements obtained by the VIRGO instrument onboard SOHO. Our reconstructions are able to reproduce variations on the time-scale of the solar rotation with much greater accuracy than previous models based on disk-integrated magnetic proxies.

**Key words:** methods: data analysis – Sun: activity – Sun: faculae, plages – Sun: magnetic fields – Sun: sunspots

## 1. Introduction

The aim of the present paper is to bring us a step closer to answering the following question: To what extent is the observed variation of solar brightness due to the evolution of the magnetic field at the solar surface? The magnetic field at the solar surface can be measured directly. The field detected in routinely obtained magnetograms is almost exclusively bundled into discrete elements of concentrated flux, often referred to as magnetic flux tubes, which cover only a small fraction of the solar surface. One major contention is that the total solar brightness is given by the (time independent) brightness of the non-magnetic solar surface (quiet Sun) and the brightness of the flux tubes whose number and distribution on the Sun is constantly evolving. Flux tubes span a whole spectrum of sizes, ranging from sunspots (20–60 Mm in diameter) to features below the best

currently obtainable spatial resolution ( $\lesssim 200$  km in diameter). The brightness signature of magnetic features is a strong function of their size: Sunspots are dark, small flux tubes are generally bright. Groups of them are seen on the solar disk as faculae or enhanced network. Whereas the brightness and thermal structure of sunspots have been well studied (see Maltby 1992 and Solanki 1997 for reviews), our knowledge of the true brightness of small-scale magnetic features is hampered by the often insufficient spatial resolution of current observations.

Within the flux-tube picture of the magnetic field (for which there is considerable support, see Solanki 1993), the average brightness of solar magnetic features is mainly a function of only two parameters: the size of the magnetic feature and its position on the Sun. Other parameters, such as the inclination to the vertical, the strength of the internal dynamics, the interaction with the neighboring granules, the phase of their evolution etc., can produce considerable variation from one magnetic feature to another, but when averaged over a sufficient number, they are expected to be of secondary importance for our purposes. Actually, our reconstructions can be used to test whether this assumption is justified. For observations that cannot resolve individual small flux tubes (and the full-disk maps used in this study are of this type), the flux-tube size can be replaced by the magnetic filling factor which is simply the fraction of the solar surface within a given pixel of the map covered by magnetic flux tubes. Solar irradiance variations are then basically explained by the changing surface area coverage and distribution of magnetic features like sunspots and faculae.

In Fligge et al. (1998; henceforth referred to as Paper I) we used disk-integrated proxies of solar magnetic features to follow the temporal behavior of sunspots and faculae. Their brightness signatures were modelled using flux spectra. Obviously, such a model cannot take into account the center-to-limb variation (CLV) of sunspot and facular contrast and hence is not able to provide satisfactory reconstructions of irradiance variations on time-scales of the solar rotation. On longer time-scales the quality of the reconstruction is better. The importance of the surface distribution of faculae for the rotational modulation of solar irradiance has been convincingly demonstrated by Lean et al. (1998).

---

Send offprint requests to: M. Fligge

In this paper we replace the one-dimensional proxies used in Paper I by full-disk magnetograms. Detailed calculations of sunspot and facular contrasts as a function of wavelength and limb distance are used (Unruh et al. 1999; henceforth referred to as Paper II) to convert magnetograms of the full solar disk into brightness maps. The irradiance is then determined by simply adding together the brightness values of all the pixels (note that only the contrast, i.e. the brightness relative to some fiducial value, is required).

Our model is still based on a very simple picture of the solar surface magnetic field, which involves only two magnetic components, namely sunspots and faculae. The atmospheric models describing the quiet Sun, sunspots and faculae, respectively, are considered to be temporally invariant and independent of the size, age (evolutionary state), shape or other intrinsic property of the surface region with which they are associated. Time-variability is introduced only by the changing surface distribution of the magnetic components due to solar rotation and the evolution of active regions.

In the following we first briefly introduce our simple 3-component model of solar surface magnetism in Sect. 2. We then sketch our scheme to decompose the magnetograms into maps of sunspots and faculae in Sect. 3 and show how to calculate irradiance variations in Sect. 4. In Sect. 5 we present model calculations of total and spectral irradiance variations and compare them to measurements obtained by the Variability of Irradiance and Gravity Oscillations (VIRGO) instrument onboard the Solar and Heliospheric Observatory (SOHO) of ESA and NASA. Finally, we conclude by summarizing our results in Sect. 6.

## 2. Method

We first outline the general procedure, how, starting from a magnetogram, a value for the solar irradiance can be determined. First, intensity spectra for each single component are calculated using Kurucz's ATLAS9 spectral synthesis code and empirical model atmospheres following Paper II. Then, magnetic maps are created by decomposing the magnetograms into sunspot and facular regions. Also, the value of the magnetic flux for each pixel is converted into a corresponding filling factor, thus taking the limited resolution of the magnetogram into account. Each pixel is then replaced by a corresponding intensity value that depends on the filling factor and position on the solar disk. Finally, by summing the intensities over the full solar disk, the value for the irradiance is calculated.

There are basically two ingredients of the model which can be adjusted in order to achieve a better reproduction of the observations. Firstly, the structure of the atmospheric models can be adjusted. This mainly concerns the thermal stratification of the facular model atmosphere, which has the largest uncertainties. Secondly, the way in which the magnetogram signal is converted into filling factor also allows some freedom. Again, this applies mainly to the facular component, since for sunspots the filling factor is always taken to be unity.

### 2.1. The 3-component model

In contrast to Paper I, where we applied our 3-component model to the Sun as a star, we now consider the resolved solar disk, i.e. each solar surface element or pixel of a magnetogram, is dealt with separately. The brightness of such an element is defined by its position on the disk, the kind of surface feature it belongs to (i.e. quiet Sun, sunspots or faculae), as well as the magnetic filling factors.

It is assumed that the intensity spectra of the quiet Sun  $I^q$ , sunspots  $I^s$  and faculae  $I^f$  depend on the limb angle  $\mu = \cos(\theta)$  and wavelength  $\lambda$ , but do not otherwise change with time  $t$ . Hence, they have to be calculated only once and can then be applied to any desired time period. In contrast, sunspot and facular magnetic filling factor maps, i.e.  $\alpha_{i,j}^s(\Phi; t)$  and  $\alpha_{i,j}^f(\Phi; t)$  respectively, are time-dependent and must be determined for each epoch at which the solar irradiance is to be calculated.  $\Phi$  is the line-of-sight magnetic flux density measured by the magnetograph and  $(i, j)$  refers to the pixels of the corresponding magnetogram.

Let  $I_{i,j}^{\text{tot}}(\lambda; t)$  be the intensity at wavelength  $\lambda$  of a given element  $(i, j)$  on the solar disk at time  $t$ . It can be written as

$$I_{i,j}^{\text{tot}}(\lambda; t) = (1 - \alpha_{i,j}^s(\Phi; t) - \alpha_{i,j}^f(\Phi; t)) \cdot I^q(\mu(i, j), \lambda) + \alpha_{i,j}^s(\Phi; t) \cdot I^s(\mu(i, j), \lambda) + \alpha_{i,j}^f(\Phi; t) \cdot I^f(\mu(i, j), \lambda). \quad (1)$$

The intensities are calculated for eleven different limb angles from  $\mu = 1.0$  at disk center to the very limb at  $\mu = 0.05$  (see Paper II). To get better radial resolution we linearly interpolate the spectra on a finer grid of  $\Delta\mu = 0.01$ .

At this point we need to clarify the meaning of  $\alpha^f$  the facular filling factor which we use in our analysis, since it differs from that generally employed when interpreting polarimetric observations. In those cases a magnetic filling factor, let us call it  $\alpha^{FT}$ , is introduced to describe the surface area fraction covered by magnetic flux tubes, with the remaining area in the resolution element being field free gas, whose properties may well differ from those of the average quiet Sun due to the proximity of the flux tube (see, e.g., Schüssler & Solanki 1988 for a more detailed discussion). Since the construction of reliable empirical models of flux tubes and their close surroundings, as well as the calculation of the CLV of the emergent intensity from a combination of the two is an ongoing major research effort which is far from completion, we have chosen to use a simplified description of faculae.  $I^f$  is taken to describe the radiation emerging from a combination of both flux tubes and their surroundings, i.e. from faculae as a whole (see Paper II). However, when calculating  $I^f$  implicitly an  $\alpha^{FT}$  must be assumed. Let us call this fiducial value  $\alpha_0^{FT}$ . We know, however, that  $\alpha^{FT}$  can differ from one facular area to the next. We model this variation in a simplified manner by introducing  $\alpha^f$ . Thus  $\alpha_{i,j}^f$  is a measure of the amount by which the actual  $\alpha^{FT}$  in pixel  $(i, j)$  differs from  $\alpha_0^{FT}$ .

As an example consider an element  $(i, j)$  lying within a sunspot. This implies  $\alpha_{i,j}^s(\Phi; t) = 1$  and  $\alpha_{i,j}^f(\Phi; t) = 0$  (see Sect. 3). The intensity of such an element is then given by

$$I_{i,j}^{\text{tot}}(\lambda; t) = I^s(\mu(i, j), \lambda), \quad (2)$$

i.e. it is only determined by the model sunspot intensity at position  $\mu$ .

In the following, we outline the scheme for mapping the magnetic features and how, using these maps, total or spectral irradiance variations can be calculated.

### 3. Mapping magnetic features

A magnetograph records the magnetic flux density  $\Phi$  parallel to the line-of-sight direction. The magnetic elements, i.e. flux tubes, are preferentially perpendicular to the solar surface. This introduces foreshortening effects and causes the magnetograph signal to decrease to the level of the instrumental background noise at the very limb even if strong magnetic regions are present. To first order, this can be corrected for by dividing the pixels of the magnetogram by their corresponding  $\mu$ -values, resulting in  $\Phi/\mu = \tilde{\Phi}$ . More precise corrections would require vector-polarimetric observations, which are not available for the full solar disk on a regular basis.

Before correcting the magnetogram for foreshortening effects we apply a threshold  $\Phi_{th}$  which depends on the limb distance  $\mu$ .  $\Phi_{th}$  is set to be constant near the limb ( $\mu < \mu_{th}$ ) to avoid amplification of signals produced purely by noise. Any magnetogram signal whose absolute value is below  $\Phi_{th}$  is set to zero before proceeding with the next step. This is illustrated in Fig. 1a.  $\Phi_{th}$  equals  $\Phi_1$  (lower limit for the threshold value) for  $\mu < \mu_{th}$ . Towards the disk center  $\Phi_{th}$  increases to  $\Phi_2$  at  $\mu = 1$ . In this manner we account for the reduction in resolution of the magnetogram and the decreasing signal-to-noise ratio towards the limb. This is found in many but not all of the MDI full-disk magnetograms obtained in the periods for which we carry out the reconstruction (and for which we do not have an explanation).

The values for  $\Phi_1$  and  $\Phi_2$  are determined by the instrumental noise of the magnetograph. For full-disk magnetograms from MDI the standard deviation of the noise is about 20 Gauss. We found  $\Phi_1 = 50$  G and  $\Phi_2 = 75$  G to give satisfactory results. However, a number of noisy pixels may still remain, especially near the limb. We, therefore, apply a second filter which checks the direct neighborhood of each pixel with  $\Phi > \Phi_{th}$ . The magnetic flux of pixels that have no neighbors whose flux exceed  $\Phi_{th}$  is set to zero.

The simplicity of our model which discerns only between two types of magnetic features, i.e. sunspots and faculae, makes the creation of maps of  $\alpha^s$  and  $\alpha^f$  relatively easy. After thresholding we associate a given pixel of a magnetogram to either a sunspot or a facular region according to its measured magnetic flux density and its contrast relative to the quiet Sun in continuum intensity images recorded by MDI (almost) simultaneously. The principle is straight forward: If the magnetic flux density of pixel  $(i, j)$  is above  $\Phi_{th}(\mu(i, j))$  then the pixel is considered to lie within an active region. If the continuum intensity in this pixel is more than  $10\sigma$  lower than that of the quiet Sun at equal  $\mu$  it belongs to a sunspot, otherwise to a facular region.

Once sunspot and facular pixels are identified their value for the magnetic flux density must be converted into a corresponding value for the magnetic filling factor. Since sunspots are well

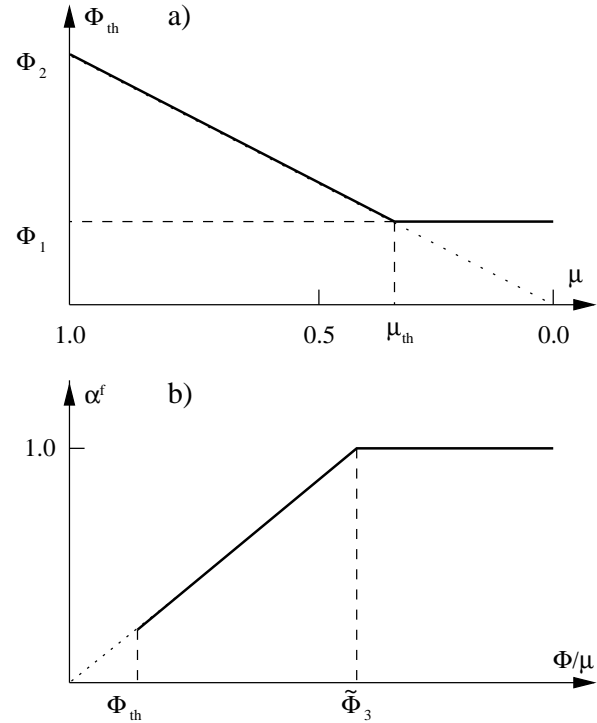


**Fig. 1.** **a** The threshold  $\Phi_{th}$  separates the signal from the noise. The  $\mu$ -dependence of  $\Phi_{th}$  accounts for the limited resolution of the magnetogram near the solar limb due to foreshortening effects and the fact that the magnetogram only records the magnetic flux in the direction of the line-of-sight.  $\Phi_{th}$  varies between  $\Phi_1$  (around disk center) and  $\Phi_2$  at the solar limb. **b** Conversion of magnetic flux  $\Phi$  measured within a pixel of a magnetogram into a corresponding facular filling factor  $\alpha^f$ .

resolved by the full-disk MDI magnetograms we employed and since stray light plays a minor role in the seeing-free environment of MDI we set the magnetic filling factor of sunspot pixels to unity, i.e.  $\alpha^s_{i,j}(\tilde{\Phi}; t) = 1$ , and everywhere else  $\alpha^s_{i,j}(\tilde{\Phi}; t) = 0$ .

Faculae are produced by weaker magnetic fields which originates from more loosely packed magnetic elements (flux-tubes). The small magnetic elements are well below the resolution of full-disk magnetograms. At least for small facular regions (with low magnetic flux density) the filling factor is smaller than 1 and an appropriate scheme which converts magnetic flux densities into filling factors must be applied.

The conversion scheme we have employed is illustrated in Fig. 1b. The facular filling factor increases linearly from zero at  $\tilde{\Phi} = 0$  to 1.0 at  $\tilde{\Phi}_3$ . Only pixels with  $\tilde{\Phi} > \Phi_{th}$  are considered. For magnetic flux densities larger than  $\tilde{\Phi}_3$ , however, the  $\alpha^f$  remains at unity. The reason for introducing this saturation lies in the observation that the average temperature enhancement within flux tubes relative to the quiet Sun decreases with increasing filling factor (Hirayama 1978, Solanki & Stenflo 1984, Solanki & Brigljevic 1992). This corresponds to a saturation of the intensity contrast with increasing filling factor. The physical reason behind this observation is that the average size of flux tubes increases with increasing magnetic filling factor (Grossmann-Doerth et al. 1994), and larger flux tubes are darker (Spruit & Zwaan 1981). Since we describe all faculae by

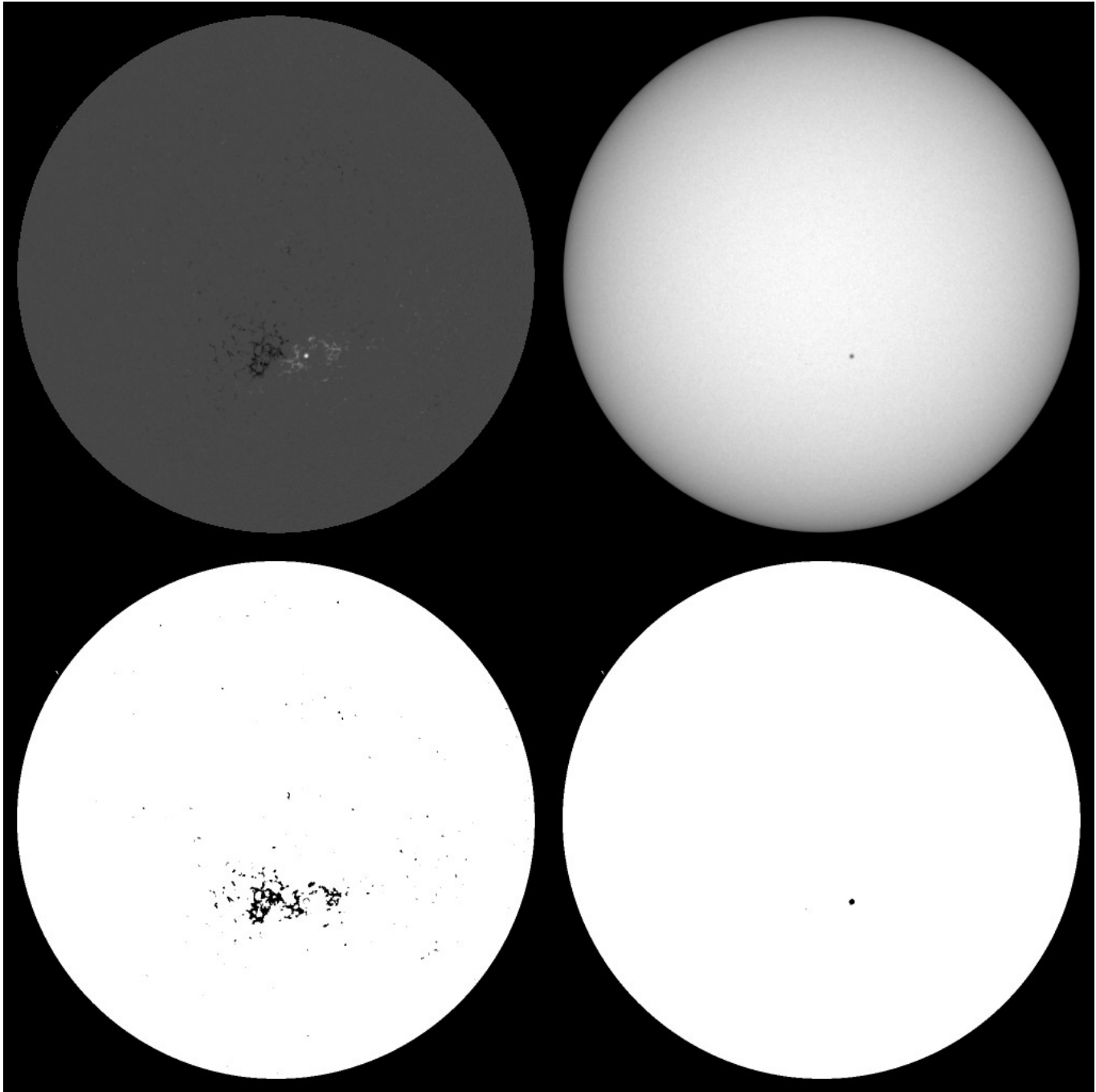


**Fig. 2.** Extraction of sunspot and facular regions from a magnetogram. The magnetogram (upper left) and the corresponding continuum intensity image (upper right) were taken on 30 August, 1996 by MDI. Below are the extracted maps for faculae (lower left) and sunspots (lower right), or more precisely  $\alpha^f$  and  $\alpha^s$ , where  $\alpha^f$  is the surface filling factor of faculae. The decaying active region visible on the solar disk is dominated by faculae, although a small spot is also present.

the same thermal structure the simplest way to account for the above observations in our model is by introducing a saturation in  $\alpha^f(\tilde{\Phi})$ . Consequently,

$$\begin{aligned} \alpha_{i,j}^f(\tilde{\Phi}; t) &= 0.0 && \text{for } \tilde{\Phi} < \Phi_{th}, \\ &= \tilde{\Phi}/\tilde{\Phi}_3 && \text{for } \Phi_{th} \leq \tilde{\Phi} \leq \tilde{\Phi}_3, \\ &= 1.0 && \text{for } \tilde{\Phi} > \tilde{\Phi}_3. \end{aligned} \quad (3)$$

$\tilde{\Phi}_3$  determines how fast the filling factor saturates as a function of magnetic flux density.  $\Phi_1$ ,  $\Phi_2$  and  $\tilde{\Phi}_3$  are free parameters and have been determined by fitting modelled irradiance variations to VIRGO measurements. The tested parameter ranges for  $\Phi_1$ ,  $\Phi_2$  and  $\tilde{\Phi}_3$  are 30–80 G, 50–200 G and 75–300 G, respectively. We find, however, that the tolerances on these parameters are considerable, e.g. around a factor of two in the case of  $\tilde{\Phi}_3$ . For

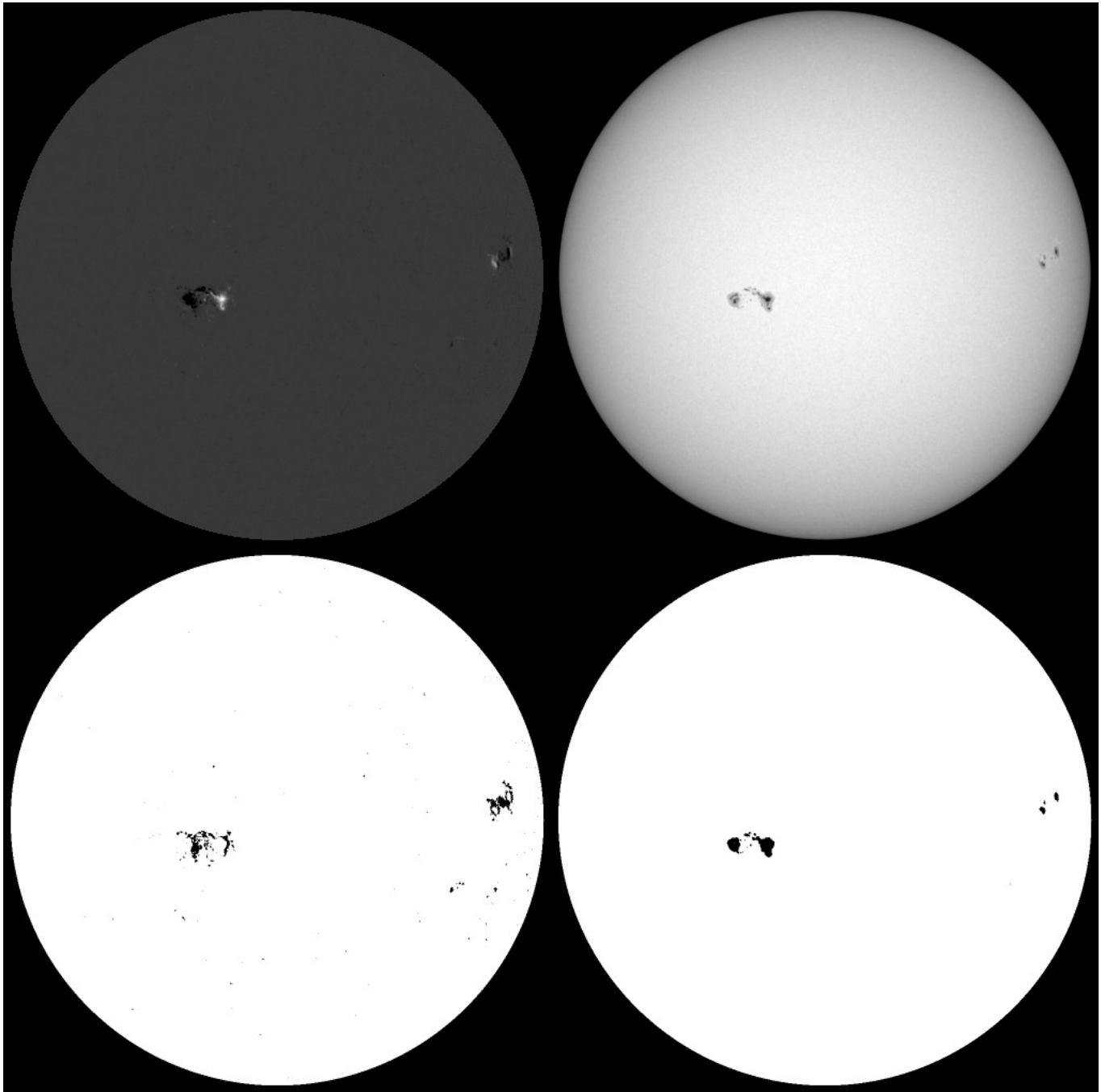


**Fig. 3.** Same as Fig. 2 but for 25 November, 1996, i.e. during the second period considered in this paper. Two active regions are present on the solar disk. The bipolar region near the center of the disk harbors the largest sunspots in VIRGO's first year of operation. The extraction works well and both facular and sunspot regions can be identified reliably. Most of the pixels far removed from these active regions that have been given  $\alpha > 0$  may be identified with ele network.

the results discussed in the following we employ  $\tilde{\Phi}_3 = 100$  G which means that already small faculae originate from densely packed magnetic elements.

The extraction of sunspots and faculae from full-disk magnetograms using the scheme outlined above is illustrated in Figs. 2 and 3. The upper two images of Fig. 2 show the magnetogram (left) and continuum intensity image (right) recorded by

MDI on 30 August, 1996. A small sunspot is present right of the solar central meridian slightly below the solar equator. The spot is surrounded by a larger facular region which, due to the low facular brightness contrast at disk center, is only seen in the magnetogram. The two lower images are the corresponding facular (left) and sunspot (right) filling factor maps, respectively. From these maps the very different morphology of sunspots and facu-

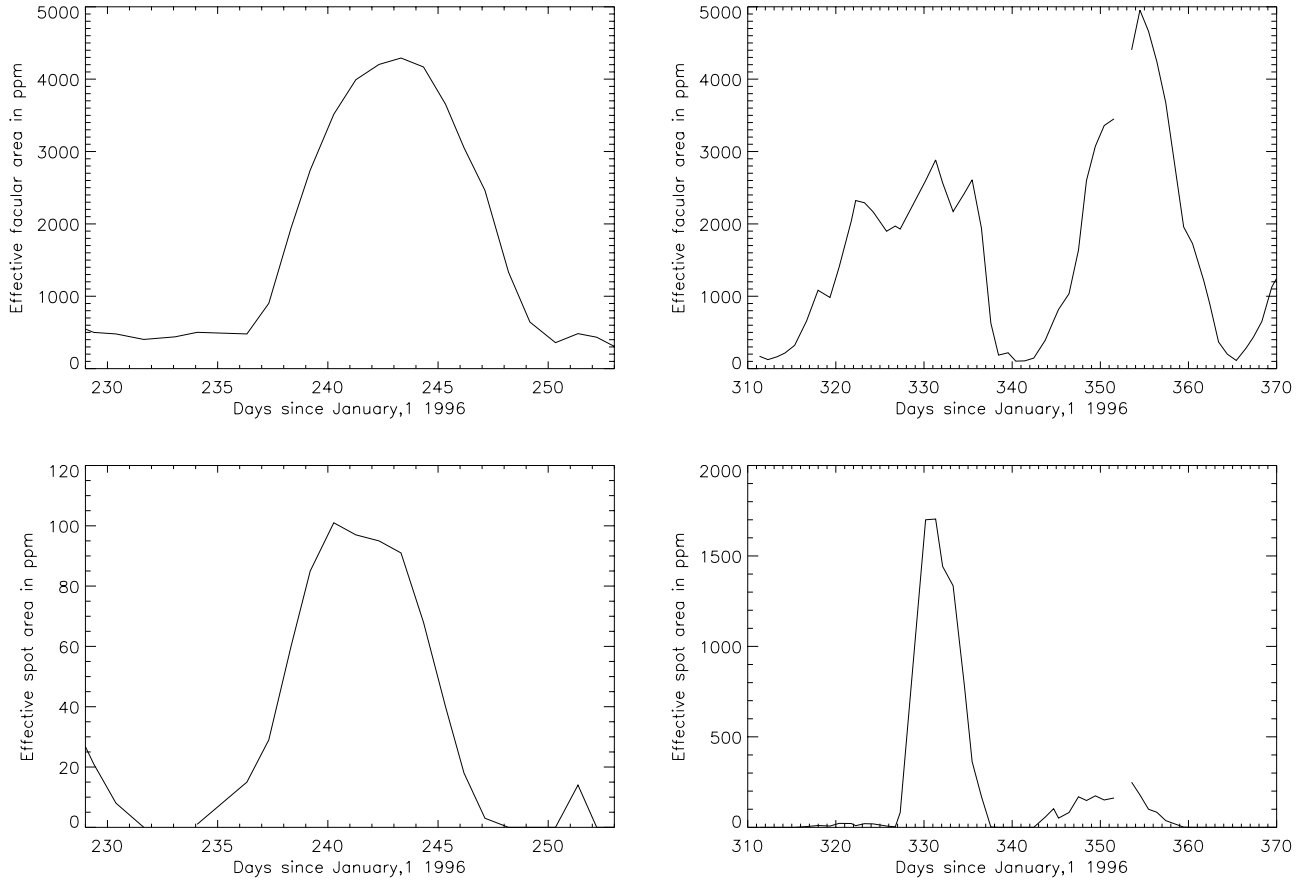


**Fig. 4.** Disk-integrated facular (upper two panels) and sunspot (lower two panels) effective areas as a function of time. Panels a) and c) correspond to the period between mid August to mid September 1996, i.e. they cover about one month, while panels b) and d) refer to the period extending from the beginning of November 1996 to the beginning of January 1997. While the facular regions have about the same size at both times, the second period has a total (effective) spot area that is over ten times larger. Some days are missing due to incomplete magnetograms.

lae becomes quite obvious. The highly structured facular region appears to be reliably extracted.

In contrast to Fig. 2, where the active region is dominated by faculae, Fig. 3 refers to a time (25 November 1996) when relatively large sunspots were present on the solar disk. Now the active regions are dominated by sunspots, although there are significant contributions from faculae too. Again, the extraction scheme reliably picks out the correct pixels for the sunspot and facular maps.

By multiplying the area covered by a pixel with the filling factors and summing over the complete solar disk, it is straight forward to determine “effective” sunspot or facular areas, respectively, i.e. the total area (in ppm) of the solar surface covered by the corresponding magnetic feature. These areas are plotted in Fig. 4 for both of the time intervals considered in this study. The two panels on the left show the variations of the effective sunspot (upper panel) and facular (lower panel) area during the first time period, i.e. between mid August and mid September 1996. The two panels on the right show the same for the second time period, i.e. between beginning of November 1996 to January 1997. When comparing the two time periods with each other, please note the different scaling of the axes.

#### 4. Calculation of irradiance variations

The solar irradiance is the total amount of radiation (per wavelength) from each point on the solar surface received on a unit area at a distance  $R$  of 1 AU aligned perpendicular to the Sun-Earth direction. Following Eq. (1) this corresponds to simply adding up  $I_{i,j}^{tot}$  over all pixels  $(i, j)$  and dividing by  $R^2$ . Since we are interested in relative irradiance variations only, we also divide by the (constant) quiet Sun contribution. As a result, the  $1/R^2$ -term cancels out. Hence, relative solar irradiance variations can be calculated according to

$$\frac{\Delta S_\lambda}{S_\lambda} = \frac{\sum_{i,j} I_{i,j}^{tot}(\lambda) - \sum_{i,j} I^q(\mu(i, j), \lambda)}{\sum_{i,j} I^q(\mu(i, j), \lambda)}. \quad (4)$$

Note that  $I^q(\mu(i, j))$  depends only on the limb angle, i.e. describes a radially symmetric image of the (quiet) Sun.

By integrating  $I_{i,j}^{tot}(\lambda)$  and  $I^q(\mu(i, j), \lambda)$  over all wavelengths total solar irradiance variations are obtained. To model VIRGO measurements (see Sect. 5) we constrain the wavelengths to the desired spectral band by multiplying the intensities  $I_{i,j}^{tot}(\lambda)$  and  $I^q(\mu(i, j), \lambda)$  with the appropriate transmission function for each of the three spectral filters prior to integration over wavelength.

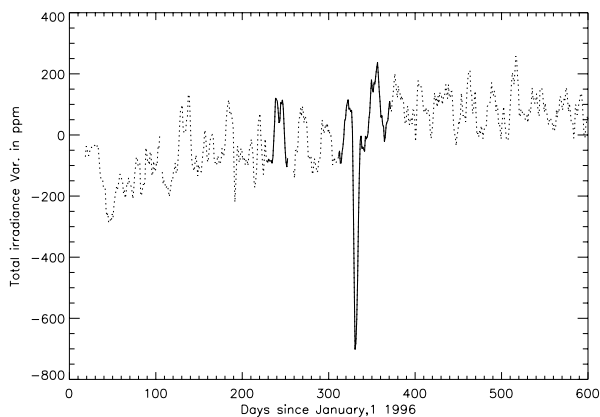


**Fig. 5.** Variability of total solar irradiance as measured by VIRGO during its first two years of operation. We reconstruct solar irradiance variations over the periods marked by the solid, thick lines.

## 5. Results

In the following, we present reconstructions of solar total and spectral irradiance variations over the two intervals 15 August 1996 – 15 September 1996 and 6 November 1996 – 6. January 1997. We compare them to VIRGO measurements of the total and the spectral irradiance at 402 nm (blue), 500 nm (green) and 862 nm (red), respectively. Fig. 5 shows the complete record of total solar irradiance variations measured during the first two years of operation (dotted line). The two periods under consideration are marked by the thick, solid line.

The magnetograms (averaged over 5 minutes and recorded every 96 minutes in the standard observing mode of MDI) are processed according to the scheme outlined in Sect. 2. Following Eqs. (1) and (4) model solar irradiance variations are calculated. We use exactly the same model configuration, i.e. atmospheric models and free parameters  $\Phi_1$ ,  $\Phi_2$  and  $\tilde{\Phi}_3$  for both time intervals.

### 5.1. August – September 1996

We first discuss the results of our calculations for the time between 15 August and 15 September 1996, i.e. days 228 to 259 of 1996. At this time the Sun was still very close to activity minimum, making it particularly suitable for a detailed study of the influence of single active regions on irradiance variations unhampered by the presence of other active regions. During this period a faculae-dominated active region harboring a small sunspot crossed the solar disk (see Fig. 2). The reconstructed (solid curve) and measured (dashed curve) irradiance variations are presented in Fig. 6. The four panels show, from top to bottom, a) total irradiance variations and spectral irradiance variations measured in the b) blue, c) green and d) red color channels of VIRGO, respectively.

The model reconstructs the observed irradiance variations relatively well. The measurements exhibit a clear spectral dependence of the contrast showing largest RMS (root-mean-square) variations in the blue channel and decreasing variability for the longer wavelength bands, which are well reproduced by

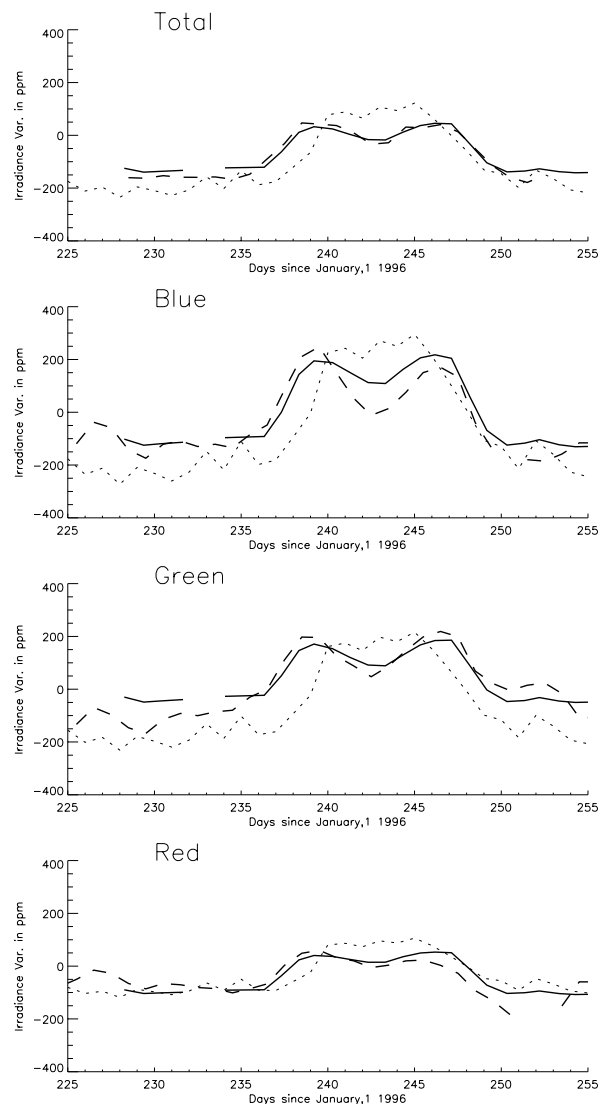


**Fig. 6.** Measured (dashed) and modelled (solid) solar total and spectral irradiance variations for the time between 15 August (day 228) and 11 September 1996 (day 255). The panels correspond to (from top to bottom) a) the total irradiance, and to the spectral irradiance variations measured in the b) blue, c) green and d) red color channels of VIRGO. Our model is able to reconstruct irradiance variations on time-scales of the solar rotation and clearly can reproduce the double-peaked structure originating from the CLV of facular brightening. However, significant deviations from the measurements remain unexplained. For comparison, the dotted curve shows the reconstruction due to Paper I, which neglected the CLV of the facular contrast.

our reconstructions. Also, the calculated RMS variations of the total irradiance are in good agreement with the measurements.

The limb brightening of faculae causes the double-peaked shape of the irradiance (seen in all channels). Near the solar limb, irradiance is increased due to the enhanced facular brightness (days 237 to 240). When the active region approaches disk center (days 240 to 243) the solar irradiance starts to decrease due to the vanishing facular contrast. This is further enhanced by the increasing influence of the spot. Then, as the region moves to the

western limb, the irradiance starts to increase again (days 243 to 247) before finally returning to the undisturbed quiet-Sun level as the region disappears behind the solar limb. This behavior is well reproduced by our model yielding linear correlation coefficients between the observed and modelled timeseries of 0.98, 0.92, 0.93 and 0.90 for the total, blue, green and red channels, respectively.

However, some discrepancy remains, mainly in the blue channel where the observations show a strong asymmetry between the left (at day 239) and the right (at day 247) irradiance peaks. The dip around day 243 predicted by the model seems to be too small compared to the observations in the blue and maybe even the green channel. Since the total and red channels do not show such deviations this may mean that the spectral dependence of the facular contrast near disk center may not yet be appropriate. On the other hand, a part of the discrepancy in individual color channels may be due to uncertainties in the correction of the long-term degradation of the individual sunphotometers. There is also a suggestion that before and after the passage of this active region the VIRGO data fluctuate more than the model. Some of this difference may have to do with the limited sensitivity of the magnetograms, so that the evolution of smaller facular features may be missed.

The importance of using full-disk maps of magnetic flux or of one of its proxies is also demonstrated in Fig. 6. The dotted curve is the reconstruction published in Paper I and is based on the disk-integrated Mg II core-to-wing ratio and the use of flux spectra to represent the quiet Sun, sunspots and facular contributions. Quite clearly, the new reconstruction, based on magnetograms and the CLV of intensity spectra is far superior. It is noteworthy that the irradiance variations never fall below the quiet Sun level even when the active region lies close to disk center, and in spite of the presence of a small sunspot. This means that, at least for the broad wavelength bands considered here, the facular contrast does not vanish at disk center which was earlier pointed out by Fröhlich et al. (1997).

Taking into account the rather sketchy picture of the solar surface magnetism which underlies our model, the differences between the measurements and reconstructions are, in our opinion, within the expected error range.

### 5.2. November 1996 – January 1997

Irradiance reconstructions for the period between the beginning of November 1996 and January 1997 are presented in Fig. 7, which is otherwise the same as Fig. 6. During this time mainly two (spatially well separated) active regions were discernible on the solar disk (see Fig. 3). They were sufficiently separated in longitude to produce two distinct features in the solar irradiance record. The first region, clearly dominated by large sunspots, causes the solar irradiance to decrease by about 1000 ppm relative to the quiet-Sun value. It crossed the solar disk between day 325 and 340. The second region, which is dominated by faculae, appears around day 345 to 360 and shows a similar behavior as the region discussed in Sect. 5.1. Again, there are two peaks in

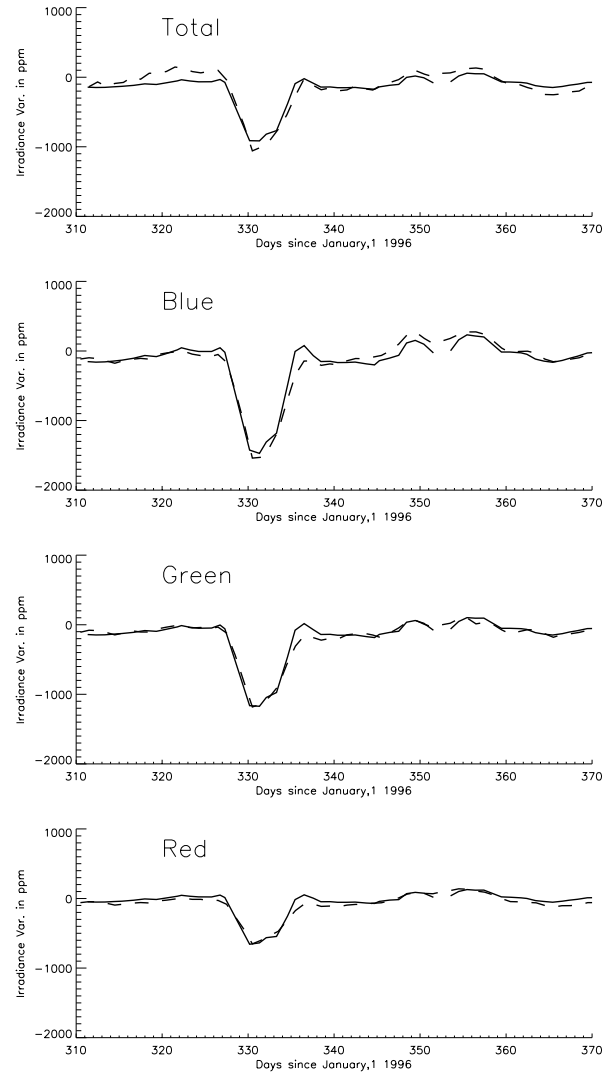


**Fig. 7.** Same as Fig. 6 but for the period between 6 November 1996 and 6 January 1997. The observed signals (dashed) of both, the spot-dominated (around day 330) and the faculae-dominated (around day 355) active regions are well reproduced by our model (solid). The same input model atmospheres and free parameters are used as in Fig. 6.

the solar irradiance time series with a dip in irradiance when the region is close to the disk center.

Again, our model is able to reproduce the measured irradiance variations for both, the spot- and the faculae-dominated regions relatively well. The linear correlation coefficients of 0.95, 0.98, 0.98 and 0.97 for the total, blue, green and red channels, respectively, are again very high. As for the first period, however, there are differences which require a closer look. One is the relatively strong increase due to facular limb brightening exhibited by the model as the first (spot-dominated) active region approaches the western solar limb (around day 336), which is not present in the observations. It is most pronounced in the blue and green channels. This may be explained by the reduced reliability of the magnetograms near the solar limb, where each magnetogram pixel

averages over a huge area on the solar surface and noise becomes a problem. In addition, the contrast calculations are also less reliable at the limb.

## 6. Summary and conclusions

We present a model of solar total and spectral irradiance variations based on a 3-component model which includes center-to-limb variations of the brightness of magnetic features. It is, to our knowledge, the first model to make direct use of magnetic maps (together with calculated intensity spectra) to reconstruct irradiance, rather than proxies such as Ca II K, Mg II k or He I 10830 Å radiation which are formed in chromospheric layers. These layers are dominated by rather different physical processes than the photospheric layers from which most of the radiation contributing to the total solar irradiance (and the three VIRGO color channels) arises. This requires detailed calculations of intensity spectra for each of the three atmospheric components as a function of wavelength and limb angle described in Paper II. This approach is able to significantly improve reconstructions of irradiance variations on time-scales of the solar rotation relative to models based on disk-integrated proxies. The good agreement between the calculated and observed CLV of the facular contrast also puts our model on a firm basis.

We wish to point out that spectra from the same atmospheric models of quiet Sun, sunspots and faculae as we use, also reproduce a number of other observations, such as the variation of the UV spectral irradiance between solar minimum and maximum, the ratio of facular to spot area, the fraction of irradiance variations due to line blanketing, etc. (see Paper II for more details).

The success of our model further strengthens the hypothesis that the magnetic field is the dominant driver of solar irradiation variations, at least on the time-scales considered. In order to further fine-tune the input parameters of our model, increase the statistical significance of the reconstructions and test our basic assumptions, longer time periods have to be considered which, preferentially, should cover different levels of solar activity.

This leaves us with the basic question whether the remaining differences between the models and the observations visible in Figs. 6 and 7 can be wiped out by taking into account more precisely the characteristics of the different surface magnetic features, i.e. following the approach taken by Harvey & White (1999), cf. Fontenla et al. (1999), or whether there are other contributors to irradiance variations of non-magnetic or only indirect magnetic origin. These questions are even more pressing on longer time-scales, which we have not addressed here.

A logical next step is to use the techniques outlined here to reconstruct a longer time series of total and spectral irradiance.

In addition to that we must consider further improvements to the models and the underlying data. Of obvious advantage would be more reliable information on the magnetic flux close to the solar limb. Full-disk vector magnetograms would be worth testing in this context. One part of our model which certainly should be improved is the connection between magnetic filling factor and spectrum in faculae. As the filling factor increases the temperature within magnetic flux tubes decreases. We take this effect extremely crudely into account. In reality, the temperature is not just lowered equally at all heights, but mainly in the deepest layers (Solanki & Brigljević 1992, Bruls & Solanki 1993). This means that the spectral shape of the emergent radiation changes. This effect needs to be taken into account. The influence of pores, dark features which may go undetected in white-light images and may thus be wrongly assigned to bright faculae, is also unclear.

*Acknowledgements.* This work was supported by the Swiss Nationalfonds under NF grant No. 2000-046894.96 and the Austrian Science foundation under grant No. S7302.

## References

- Bruls J.H.M.J., Solanki S.K., 1993, A&A 273, 293
- Fligge M., Solanki S.K., Unruh Y.C., Fröhlich C., Wehrli Ch., 1998, A&A 335, 709
- Fontenla J., White O.R., Fox P.A., Avrett E.H., Kurucz R.L., 1999, ApJ 518, 480
- Fröhlich C., Andersen B., Appourchaux T. et al., 1997, Solar Phys. 170, 1
- Grossmann-Doerth U., Knölker, M., Schüssler M., Solanki S.K., 1994, A&A 285, 648
- Harvey K.L., White O.R., 1999, ApJ 515, 812
- Hirayama T., 1978, PASJ 30, 337
- Lean J.L., Cook J., Marquette W., Johannesson A., 1998, ApJ 492, 390
- Maltby P., 1992, In: Thomas J.H., Weiss N.O. (eds.) Sunspots: Theory and Observations. Kluwer, Dordrecht, p. 103
- Schüssler M., Solanki S.K., 1988, A&A 192, 338
- Solanki S.K., 1993, Space Sci. Rev. 61, 1
- Solanki S.K., 1997, In: Schmieder B., del Toro Iniesta J.C., Vázquez M. (eds.) Advances in the Physics of Sunspots. ASP Conf. Ser. Vol. 118, p. 178
- Solanki S.K., Brigljević V., 1992, A&A 262, L29
- Solanki S.K., Stenflo J.O., 1984, A&A 140, 185
- Spruit H.C., Zwaan C., 1981, Solar Phys. 70, 207
- Unruh Y.C., Solanki S.K., Fligge M., 1999, A&A 345, 635